Infill Density in Additive Manufacturing and Application to the DFMA of an Iron Man Helmet

Rajan Vraitch
Mechanical, Biomedical and Design Engineering, Aston University
Birmingham, UK
190073822@aston.ac.uk

Mark Prince
Mechanical, Biomedical and Design Engineering, Aston University
Birmingham, UK
m.prince1@aston.ac.uk

Jean-Baptiste R. G. Souppez
Mechanical, Biomedical and Design Engineering, Aston University
Birmingham, UK
j.souppez@aston.ac.uk

***Abstract*—Additive manufacturing has become increasingly popular for rapid prototyping and industrial applications, particularly in the context of Industry 4.0. However, given the vast design parameter space, there remains a lack of characterisation of the mechanical properties for varying design parameters. Consequently, flexural tests are undertaken following the ISO 178:2019 for fused deposition modelling (FDM) samples, with three infill patterns (lines, gyroid and triangles), four thermoplastic materials, namely acrylonitrile butadiene styrene (ABS), polylactic acid (PLA and PLA+), and polyethylene terephthalate glycol (PETG), and infill densities (print material to part volume ratio) ranging from 0.10 to 1.00. Here we show that (i) the modulus and strength are independent of the tested infill types; (ii) the mechanical properties increase linearly with infill density; and (iii) considering mechanical properties, mass and cost, PLA+ appears as the most suitable overall material choice, with PETG appropriate for strength-driven, low-cost applications. Ultimately, PLA+ is applied to the design for manufacturing and assembly (DFMA) case study of an Iron Man helmet. These findings provide novel insights into the variations of mechanical properties with infill type, density and material for 3D printing applications and may contribute to future development in lightweight and cost-effective additive manufacturing.**

***Index Terms*—Additive Manufacturing, 3D Printing, Industry 4.0, Design for Manufacture and Assembly, Mechanical Testing**

I. Introduction

Additive manufacturing (AM) processes, widely recognised as 3D printing, have been increasingly employed for industrial applications and are central to the fourth industrial revolution, Industry 4.0 [1], [2]. AM has proven faster [3], more cost-effective [4] and more sustainable [5] than subtractive manufacturing (SM), particularly for highly complex, low volume components [6]. Consequently, AM has been employed in industries ranging from aerospace [7] to medical devices [8]. Indeed, the ability to produce complex geometries at a cheaper and faster rate than SM has led to new advances in the biomedical field, including patient-specific spinal implants [9].

However, much remains to be understood on the impact of design variables on the mechanical properties of 3D printed components. Infill density has been identified as a critical factor in additive manufacturing [10], particularly for fused deposition modelling (FDM) components due to its common use in AM [11]. The experimental characterisation of tensile and compressive properties [12] has received comparatively more attention than flexural properties [13].

Consequently, this paper explores the effect of three infill types and four materials at various infill densities on the flexural properties of FDM samples. The aim is to offer insights into material selection and design for manufacturing and assembly (DFMA), thereby enhancing the performance of 3D printed parts whilst optimising manufacturing efficiency.

The remainder of this paper is structured as follows. Section II details the experimental methodology employed, including the materials and manufacturing of the samples, the experimental setup and quantification of mechanical properties, and associated uncertainties. Section III then presents the results of the 3-point bend tests. Subsequently, Section IV applies the findings to a case study of an Iron Man helmet. Finally, Section V summarises the main results of this study.

II. Methodology

A. Materials and Manufacturing

The geometric definition of the test samples follow the ISO 178:2019 [14], namely a length $L = 80 \pm 2\,\mathrm{mm}$, width $b = 10 \pm 0.2\,\mathrm{mm}$ and thickness $h = 4 \pm 0.2\,\mathrm{mm}$. This ensures the mechanical properties ascertained are reliable and repeatable and can be employed for design purposes. All samples were manufactured using a Creality Ender 3 Max Neo FDM 3D printer. FDM was adopted as it is the most common AM process [11]. It utilises the geometrical conditions imported from a stereolithography (STL) file to horizontally deposit a molten wire filament drawn through a motorised pulling system, where the filament passes through a heated liquefier set at a temperature above the materials melting point, causing the filament to melt and soften. The filament is then extruded through a nozzle head moving on the horizontal xy-plane. As the extruder moves, the molten filament is laid down onto the printing platform, which moves vertically along the z-axis to form the 3-dimensional geometry layer by layer.

The printing parameters were kept constant to maintain consistency across all samples. The print speed was 50 mm s^{-1}, and the layer height 0.20 mm. Moreover, the print and mechanical testing orientation was identical for all samples. Printing temperatures were slightly adjusted to facilitate the extrusion of each specific material. The material properties, specific print parameters inherent to each material, as well as the achieved sample sizes, are characterised in Table I.

TABLE I
PRINT PARAMETERS AND RESULTING GEOMETRIC SAMPLE SIZES

Parameter	***Material***			
	ABS	PLA	PLA+	PETG
Cost, C_m [GBP kg^{-1}]	18.99	18.99	17.99	16.99
Density, ρ [kg m^{-3}]	1050	1240	1260	1230
Nozzle temperature [°C]	240	210	210	230
Platform temperature [°C]	90	60	60	80
Number of perimeter walls	2	4	4	2
Perimeter wall thickness [mm]	1.60	0.80	0.80	1.60
Width, b [mm]	10.18 ± 0.022	10.08 ± 0.038	10.14 ± 0.044	10.18 ± 0.016
Thickness, h [mm]	4.15 ± 0.018	3.97 ± 0.044	4.08 ± 0.059	4.04 ± 0.049

This study employs the most common thermoplastic materials used in FDM, namely: (i) ABS (acrylonitrile butadiene styrene), characterised by its high impact and heat resistance [15]; (ii) PLA (polylactic acid), for its ease of printing [16] and low shrinkage, achieving the closest dimensions compared to the intended ones in Table I; (iii) PLA+, an enhanced version of PLA with increased strength to weight qualities [17]; and (iv) PETG (Polyethylene terephthalate glycol), a co-polymer combining the best features of PLA (low shrinkage) and ABS (high impact resistance) [18].

First, three types of infills, namely lines (Fig. 1a), gyroid (Fig. 1b) and triangles (Fig. 1c) are employed with PLA for infill densities ρ_i from 0.10 to 1.00 (solid sample) in 0.10 increments, where ρ_i is defined as the ratio of the internal printed material's volume to the part's total internal volume.

Then, samples are manufactured with a gyroid infill pattern for infill densities $\rho_i = 0.10,\ 0.25,\ 0.50,\ 0.75$ and 1.00 out of ABS, PLA, PLA+ and PETG. The variations in internal structure with infill density are illustrated in Fig. 1d-e. The gyroid pattern is a three-dimensional, triply periodic minimal surface structure [19] that provides optimal strength-to-weight ratios and efficient material usage in 3D-printed parts [20]. It also allows for better stress distribution which reduces the likelihood of localised stress concentrations and thus improves the mechanical properties [21].

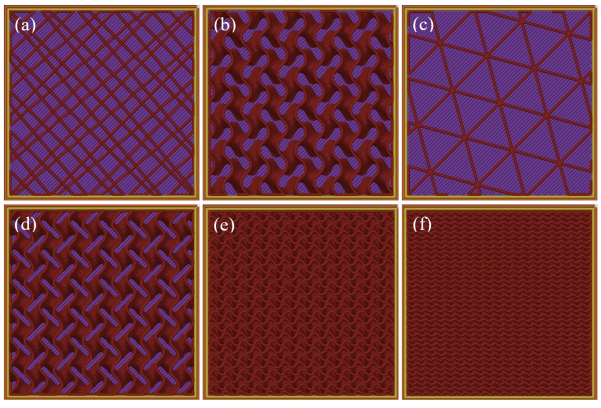

Fig. 1. Horizontal section showing infill types, namely: (a) lines, (b) gyroid, (c) triangles at $\rho_i = 0.20$, and gyroid infill at (d) $\rho_i = 0.25$, (e) $\rho_i = 0.50$, and (f) $\rho_i = 0.75$. Dark red represents 3D printed material, and violet represents empty space. The transverse y-axis corresponds to the orientation of the span in Fig. 2.

Due to their relatively poor layer adhesion capabilities, the ABS and PETG samples were manufactured with 4 perimeter walls to promote bonding between the layers, whereas PLA and PLA+ were manufactured with 2 perimeter walls as they exhibit stronger layer adhesion qualities. The overall perimeter thickness was identical for all samples.

B. Experimental Setup and Protocol

Experiments were conducted in accordance with the ISO 178:2019 [14] on a universal testing machine (Instron 5965 series) fitted with a 500 N loadcell. The apparatus and flexural (3-point bend) setup are depicted in Fig. 2, where the span between support point is $s = 64\,\mathrm{mm}$ [14]. Forces were sampled at 100 Hz, in the following environmental conditions for the temperature $18.5\,^{\circ}\mathrm{C} \leq T \leq 21.5\,^{\circ}\mathrm{C}$ and relative humidity $0.269 \leq \varphi \leq 0.377$. A 0.05 N preload is applied at a displacement rate of 1 mm min^{-1} before each test. The load is then applied at a displacement rate of 2 mm min^{-1} until failure, where failure is taken as a 20% drop in load compared to the maximum load.

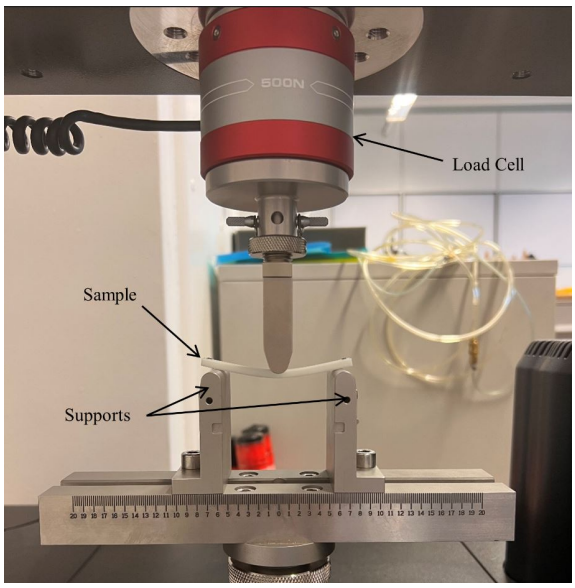

Fig. 2. Experimental setup for 3-point bend test.

C. Mechanical Properties

From the measured deflection w and force F, the flexural strain ϵ_f, flexural stress σ_f and flexural modulus E_f are computed using equations (1), (2) and (3), respectively. E_f is computed using the linear least squares method for $0.0005 \leq \epsilon_f \leq 0.0025$.

$$\epsilon_f = \frac{6wh}{s^2} \quad (1) \qquad \sigma_f = \frac{3Fs}{2bh^2} \quad (2) \qquad E_f = \frac{\sigma_f}{\epsilon_f} \quad (3)$$

D. Uncertainty

The uncertainty U is given as the root sum of the precision A and the bias B [22], such that

$$U = \sqrt{A^2 + B^2} = \sqrt{\left(\frac{t_{95}S}{\sqrt{n}}\right)^2 + B^2}, \quad (4)$$

where $t_{95} = 2.776$ for $n = 5$ at the 95% confidence level, and S is the standard deviation of the average results. Five repeats were undertaken, in line with the ISO 178:2019 [14]. The experimental bias limits B are $B(F) = 0.000\,05\,\text{N}$, $B(b) = B(h) = B(s) = 0.005\,\text{mm}$ and $B(w) = 0.000\,05\,\text{mm}$, respectively. The uncertainty will be presented as vertical error bars throughout Section III.

III. Results

A. Infill Type

The flexural modulus E_f and ultimate flexural strength σ_{uf} of PLA samples with varying infill patterns (lines, gyroid and triangles) for $0.10 \leq \rho_i \leq 1.00$ are presented in Fig. 3. For the infill patterns tested, both the stiffness and strength are shown to be independent of the infill pattern. It is noted that σ_{uf} for the PLA samples with triangles infill deviates from the lines and gyroid trend for $\rho_i \geq 0.60$. The mechanical properties also linearly increase with ρ_i. The average stress-strain curves ($n = 5$) are depicted in Fig. 4.

E_f and σ_{uf} have been shown to be independent of the infill type and to increase linearly with ρ_i, even with the increased uncertainty associated with the former. Consequently, the material comparison between ABS, PLA, PLA+ and PETG will be undertaken on gyroid infill patterns only, as detailed in Section II-A, for $\rho_i = 0.10,\ 0.25,\ 0.50,\ 0.75$ and 1.00.

B. Material Selection

The ultimate flexural strength of PLA, PLA+ and PETG are of comparable magnitude and superior to that of ABS, as evidenced in Fig 5a. However, ABS also features a lower density ρ than PLA, PLA+ and PETG (Table I). Therefore, the specific mechanical properties, namely the specific flexural modulus E_f/ρ and specific ultimate flexural strength σ_{uf}/ρ are presented in Fig 5b. Even when considering its lower density, the specific strength of ABS remains comparatively lower than that of PLA, PLA+ and PETG. Interestingly, because of its lower cost C_m (Table I), PETG may prove a suitable option for strength-driven, low-cost application, as demonstrated by its high strength-cost ratio σ_{uf}/C_m.

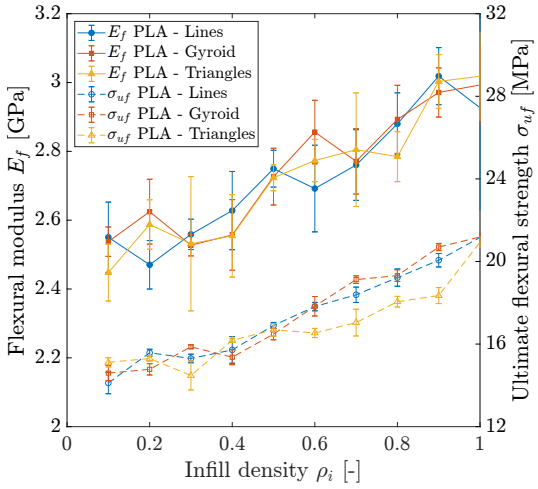

Fig. 3. Flexural modulus E_f (solid lines) and ultimate flexural strength σ_{uf} (dashed lines) for PLA with lines, gyroid and triangles infill patterns at $0.10 \leq \rho_i \leq 1.00$ ($n = 5$).

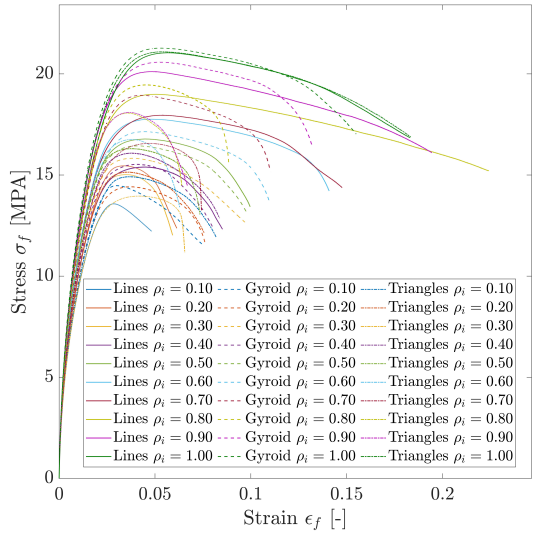

Fig. 4. Average stress-strain curves ($n = 5$) for PLA with lines (solid line), gyroid (dashed line) and triangles (dash-dotted line) infill patterns at $0.10 \leq \rho_i \leq 1.00$.

For stiffness-driven designs, the flexural modulus E_f, specific flexural modulus E_f/ρ, and modulus-cost ratio E_f/C_m of the materials are shown in Fig 5a and Fig 5b, and Fig 5c, respectively. In all cases, PLA and PLA+ appear superior to ABS and PETG, with PLA+ exhibiting the highest values of E_f, E_f/ρ and E_f/C_m at all infill densities. Consequently, PLA+ appears as the most suitable material for lightweight strength and stiffness-driven design applications.

Comparing the properties of ABS, PLA, PLA+ and PETG, also considering the effect of their density and cost, PLA+ has been identified as the most suitable candidate material for lightweight applications. However, the failure behaviour of the materials remains to be investigated.

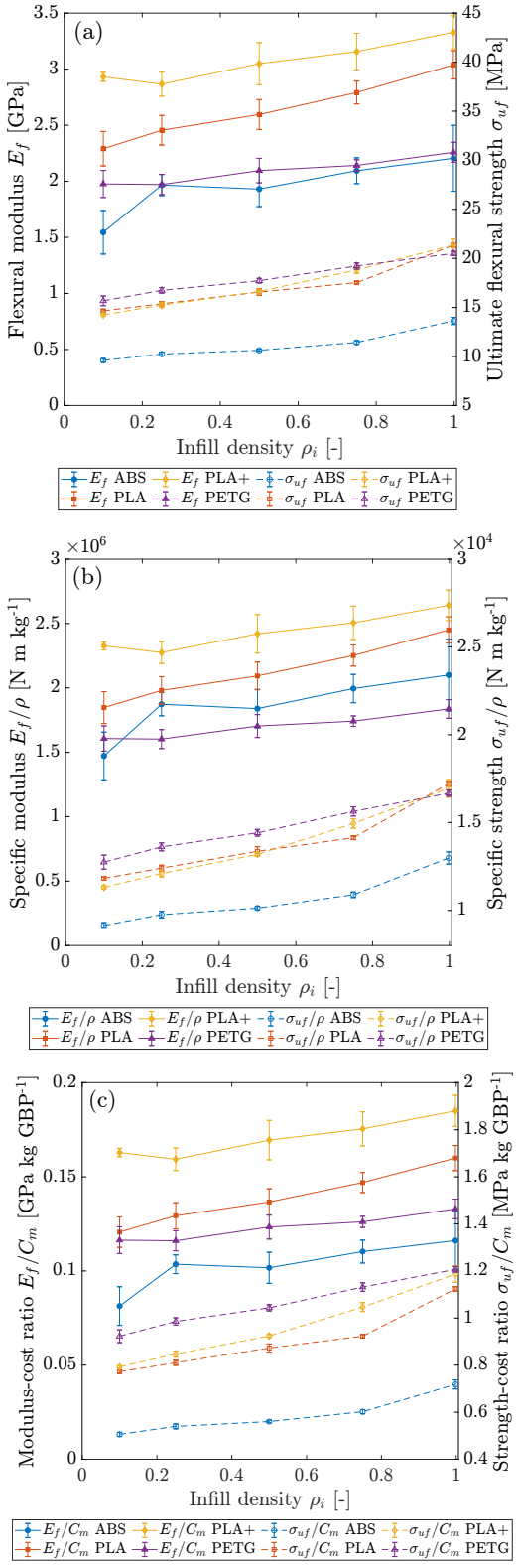

Fig. 5. (a) flexural modulus E_f (solid lines) and ultimate flexural strength σ_{uf} (dashed lines); (b) specific flexural modulus E_f/ρ (solid lines) and specific ultimate flexural strength σ_{uf}/ρ (dashed lines); and (c) modulus-cost E_f/C_m (solid lines) and strength-cost ratio σ_{uf}/C_m (dashed lines) for ABS, PLA, PLA+ and PETG at $0.10 \leq \rho_i \leq 1.00$ ($n = 5$).

C. Failure Mechanism

The average stress-strain curves of the five repeats of each experiment are presented in Fig. 6, where the stress and strain are computed as in equations (1) and (2). The comparatively lower E_f and σ_{uf} of ABS is clearly visible, as is the increase in stiffness and strength with increasing infill density. The stress-strain curves allow to characterise the failure mechanism of the samples. ABS displays a rapid fracture past its ultimate flexural strength and associated ultimate flexural strain, evidenced by the dramatic drop in the stress-strain curve. Conversely, PLA, PLA+ and PETG exhibit a large necking region prior to fracture.

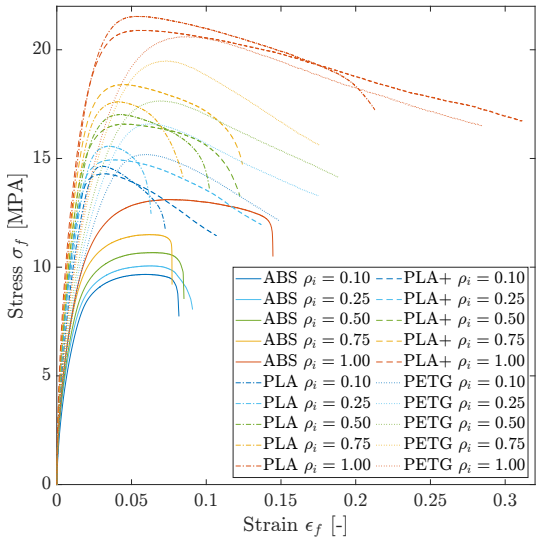

Fig. 6. Average stress-strain curves ($n = 5$) for ABS (solid line), PLA (dash-dotted line), PLA+ (dashed line) and PETG (dotted line) at $0.10 \leq \rho_i \leq 1.00$.

In Section III-A, we showed that mechanical properties are independent of the infill type, and increase linearly with the infill density. In Section III-B, we compared the mechanical properties ABS, PLA, PLA+ and PETG, and identified PLA+ as the most candidate material. Finally, in Section III-C, we characterised the failure behaviour of all materials. Therefore, PLA+ has been retained for the case study of the design for manufacturing and assembly of an Iron Man helmet, presented in Section IV.

IV. Case Study: Iron Man Helmet

This section presents the case study of the DFMA of an Iron Man helmet [23], which follows the four universal stages involved with AM, detailed in Fig. 7, and tackled in Sections IV-A, IV-B, IV-C and IV-D, respectively.

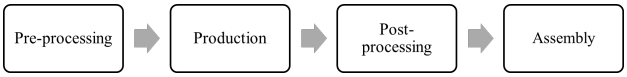

Fig. 7. Flowchart of the four universal stages of additive manufacturing.

A. Pre-Processing

Pre-processing is a crucial stage of the AM process that involves preparing 3D models [24] through careful selection of the printing parameters to optimise the quality, cost and print time of the part.

However, the 'stair-stepping' effect is a prevalent issue that is observed in FDM that stems from the layering of material, causing deviations from the desired geometry [25]. At larger layer heights, the effect is more pronounced, necessitating more extensive post-processing to achieve a smoother surface finish. To optimise the post-processing duration whilst also enhancing the accuracy between the printed geometry and its desired geometry, a reduced layer height of 0.08 mm was employed. PLA+ with a 0.20 infill density using a gyroid pattern was utilised, informed by the results from Section III, to achieve the necessary strength and stiffness while minimising print time and material, and thus cost.

The selection of the printing orientation is a crucial factor that has been carefully considered to optimise the material usage and printing time whilst reducing the 'stair-stepping' effect [26]. Through the strategic orientation of each part, the overall manufacturing times were optimised, which ultimately decreased the overall production cost. The significant influence of the printing orientation is exemplified through the helmet's faceplate where opting for an upright (Fig. 8a) rather than flat orientation (Fig. 8b) the following are achieved:

- A 57.8% reduction in print material was achieved in the upright orientation, using 150.67 g compared to 356.42 g. This also directly translates into a 57.8% savings in material cost, consistent with previous studies [27].
- A 56.3% reduction in print time, completed in 4 hours 40 minutes compared to 10 hours 41 minutes if printed flat, thus enhancing the overall efficiency of the process.
- The visibility of layer lines on the faceplate's surface was reduced (Fig. 8), thereby reducing the post-processing time needed for sanding and finishing.

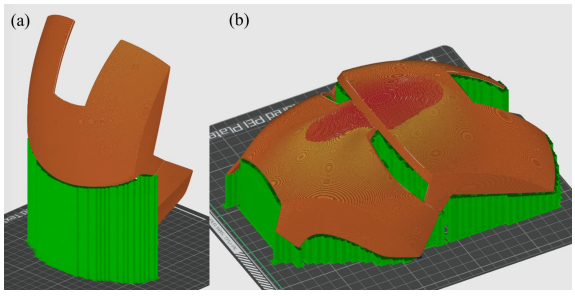

Fig. 8. Effects of part orientation on support material (green) for (a) upright and (b) flat print orientations.

This approach demonstrates the importance of strategic part orientation in 3D printing, as it directly impacts the overall quality, resource efficiency, and ease of post-processing for the final product.

B. Production

In the production stage, the digital 3D model is transformed into a tool path, which is then executed by the 3D printer. The tool path outlines the precise coordinates and the deposition rate for each layer, ensuring that the printer nozzle accurately follows the geometry for the 3D model. Here, all print parameters remain identical to the PLA+ printing parameters of the test samples, previously detailed in Table I, with the exception of the layer height as discussed in Section IV-A.

C. Post-Processing

Although AM provides many advantages over other manufacturing methods, such as SM, due to the stair-stepping effect highlighted in Section IV-A, one drawback of FDM is that a rough surface finish is produced. To achieve a smooth surface, the parts were therefore sanded, initially with 100 grit sandpaper once the supports were removed [28]. The process was then repeated, using progressively finer grades of sandpaper, down to 1000 grit wet and dry sandpaper. Spray primer was then carefully applied to prepare the surface for painting. Subsequently, thin layers of spray paint were applied with a final, gentle wet sanding using 2500 grit before administering the final coat of spray paint. Eventually, a smooth and aesthetically appealing surface was achieved.

D. Assembly

The concluding stage involves the assembly of the various printed components to form the final Iron Man helmet. This entails ensuring the precise alignment and fit of the parts whilst adhering to the required tolerances and design specifications.

The use of standard-sized fasteners facilitated an optimal assembly time, which not only improved the helmet's overall structural rigidity but also reduced the overall manufacturing cost by eliminating the need for custom fasteners. Additionally, plastic soldering of excess waste support material was recycled to create an internal joint seam that further reinforced the bond between various components. To enhance the helmet's ergonomics, padded foam was also added to the interior of the helmet through adhesive bonding, providing additional support and cushioning for enhanced user comfort.

Ultimately, the assembly combined the various individual components to create a functional and visually appealing finished product which is depicted in Fig. 9.

V. Conclusions

Flexural (3-point bend) tests have been undertaken in accordance with the ISO 178:2019 on FDM-manufactured PLA samples with lines, gyroid and triangles infill patterns at infill density from 0.10 to 1.00 in 0.10 increments. Moreover, gyroid samples manufactured from ABS, PLA, PLA+ and PETG at infill densities of 0.10, 0.25, 0.50, 0.75 and 1.00.

On the PLA samples, the infill patterns tested did not prove to yield any significant differences in mechanical properties, thus suggesting that the stiffness and strength is independent of the infill pattern. Additionally, the results evidence a linear increase in mechanical properties with the infill density.

Fig. 9. Final Iron Man helmet.

The comparison of mechanical properties for ABS, PLA, PLA+ and PETG revealed a comparatively lower stiffness and strength for ABS, as well as fracture occurring rapidly after the ultimate strength is reached. This is in contrast with PLA, PLA+ and PETG. While the latter may prove to be appropriate for solely strength-driven, low-cost applications, PLA+ is the most appropriate and versatile option.

Consequently, it was employed for the case study of an Iron Man helmet. This practical application of additive manufacturing, informed by the experimental results, evidenced crucial elements in the design for manufacturing and assembly of 3D printed parts, with 57.8% material and 56.3% time savings achieve solely by optimising the face plate print orientation.

These results offer novel insights into the mechanical properties of common materials employed with FDM, for varying infill patterns, infill densities and materials. It is anticipated these findings may contribute to future development in lightweight and cost- effective additive manufacturing, and applications ranging from aerospace to medical implants.

REFERENCES

[1] U. M. Dilberoglu, B. Gharehpapagh, U. Yaman, and M. Dolen. “The role of additive manufacturing in the era of industry 4.0”, Procedia Manufacturing, vol. 11, pp.545-554, 2017.

[2] L. Boyd, Y. Lu, and J.-B. R. G. Souppez. “Pedagogy 4.0: Employability skills and computer aided design (CAD) education for Industry 4.0”, The 28th International Conference on Automation and Computing (ICAC2023), Birmingham, UK, 30/08-01/09/2023, 2023.

[3] G. Manogharan, R. A. Wysk, R.A. and O. L. Harrysson. “Additive manufacturing–integrated hybrid manufacturing and subtractive processes: economic model and analysis”, International Journal of Computer Integrated Manufacturing, vol. 29(5), pp.473-488, 2016.

[4] O. A. Mohamed, S. H. Masood, and J. L. Bhowmik. “Optimization of fused deposition modeling process parameters for dimensional accuracy using I-optimality criterion”, Measurement, vol. 81, pp.174-196, 2016.

[5] L. S. R. Krishna, and P. J. Srikanth. “Evaluation of environmental impact of additive and subtractive manufacturing processes for sustainable manufacturing”, Materials Today: Proceedings, vol. 45, 2021.

[6] H. Paris, H. Mokhtarian, E. Coatanéa, M. Museau, and I. F. Ituarte. “Comparative environmental impacts of additive and subtractive manufacturing technologies”, CIRP Annals, vol. 65(1), pp.29-32, 2016.

[7] B. Lyons. “Additive manufacturing in aerospace: Examples and research outlook”, The Bridge, vol. 44(3), 2014.

[8] A. George, M. Prince, and C. Coulson. “Safe nasendoscopy assisted procedure in the post-COVID-19 pandemic era”, Clinical Otolaryngology, vol. 45(5), p.844, 2020.

[9] J. L. Burnard, W. C. Parr, W. J. Choy, W. R. Walsh, and R. J. Mobbs. “3D-printed spine surgery implants: a systematic review of the efficacy and clinical safety profile of patient-specific and off-the-shelf devices”, European Spine Journal, vol. 29, pp.1248-1260, 2020.

[10] M. Samykano. “Mechanical property and prediction model for FDM-3D printed polylactic acid (PLA)”, Arabian Journal for Science and Engineering, vol. 46, pp.7875-7892, 2021.

[11] M. Lalegani Dezaki, M. K. A. Mohd Ariffin, and S. Hatami. “An overview of fused deposition modelling (FDM): Research, development and process optimisation”, Rapid Prototyping Journal, vol. 27(3), pp.562-582, 2021.

[12] S. H. Ahn, M. Montero, D. Odell, S. Roundy and P. K. Wright. “Anisotropic material properties of fused deposition modeling ABS”, Rapid Prototyping Journal, 2002

[13] M. T. Birosz, D. Ledenyák and M. Ando, M. “Effect of FDM infill patterns on mechanical properties”, Polymer Testing, vol. 113, 2022.

[14] International Organization for Standardization. “ISO 178:2019 Plastics - Determination of flexural properties”, International Organization for Standardization, Geneva, Switzerland, 2019.

[15] H. García-Martínez, E. Ávila-Navarro, G. Torregrosa-Penalva, A. Rodríguez-Martínez, C. Blanco-Angulo and M. A. de la Casa-Lillo. “Low-cost additive manufacturing techniques applied to the design of planar microwave circuits by fused deposition modeling”, Polymers, vol. 12(9), p.1946, 2020.

[16] E. H. Baran, and H. Y. Erbil. “Surface modification of 3D printed PLA objects by fused deposition modeling: a review”, Colloids and Interfaces, vol. 3(2), p.43, 2019.

[17] M. Baraheni, M. R. Shabgard and S. Amini. “Evaluating the hole quality produced by vibratory drilling: additive manufactured PLA+”, The International Journal of Advanced Manufacturing Technology, vol. 117(3-4), pp.785-794, 2021.

[18] K. Durgashyam, M. I. Reddy, A. Balakrishna and K. Satyanarayana, K. “Experimental investigation on mechanical properties of PETG material processed by fused deposition modeling method”, Materials Today: Proceedings, vol. 18, pp.2052-2059, 2019.

[19] P. Bean, R. A. Lopez-Anido and S. Vel. “Numerical modeling and experimental investigation of effective elastic properties of the 3D printed gyroid infill”, Applied Sciences, vol. 12(4), p.2180, 2022.

[20] A. Yánez, A. Herrera, O. Martel, D. Monopoli, and H. Afonso. “Compressive behaviour of gyroid lattice structures for human cancellous bone implant applications”, Materials Science and Engineering, vol. 68, pp.445-448, 2016.

[21] D. W. Abueidda, W. Elhebeary, C. S. A. Shiang, S. Pang, R. K. A. Al-Rub and I. M. Jasiuk. “Mechanical properties of 3D printed polymeric Gyroid cellular structures: Experimental and finite element study”, Materials and Design, vol. 165, p.107597, 2019.

[22] J.-B R. G. Souppez, and J. Laci. “Ultimate strength of quasi-isotropic composites: ISO 12215-5:2019 validation”, The Royal Institution of Naval Architects Part A: International Journal of Marine Engineering, vol. 162(A), pp.237-246, 2022.

[23] R. Vraitch. “DFMA of a 3D printed Iron Man helmet”, Aston University Final Year Dissertation, 2023.

[24] A. Mathew, S. R. Kishore, A. T. Tomy, M. Sugavaneswaran, S. G. Scholz, A. Elkaseer, V. H. Wilson, A. J. Rajan, “Vapour polishing of fused deposition modelling (FDM) parts: a critical review of different techniques, and subsequent surface finish and mechanical properties of the post-processed 3D-printed parts”, Progress in Additive Manufacturing, pp.1-18, 2023.

[25] F. M. Mwema, and E. T. Akinlabi. Basics of fused deposition modelling (FDM). Fused deposition modeling: strategies for quality enhancement”, National Library of Medicine, pp.1-15, 2020.

[26] M. A. Matos, A. M. A. Rocha, and A. I. Pereira. “Improving additive manufacturing performance by build orientation optimization”, The International Journal of Advanced Manufacturing Technology, 107, pp.1993-2005, 2020.

[27] G. Boothroyd. ”Product design for manufacture and assembly.” Computer-Aided Design vol. 26(7), pp.505-520, 1994.

[28] J. R. C. Dizon, C. C. L. Gache, H. M. S. Cascolan, L. T. Cancino, and R. C. Advincula. “Post-processing of 3D-printed polymers”, Technologies, 9(3), p.61, 2021.